Final Draft

of the original manuscript

Sun, Y.; Helmholz, H.; Will, O.; Damm, T.; Wiese, B.; Luczak, M.; Peschke, E.; Luthringer-Feyerabend, B.; Ebel, T.; Hövener, J.; Glüer, C.; Willumeit-Römer, R.:

Dynamic in vivo monitoring of fracture healing process in response to magnesium implant with multimodal imaging: Pilot longitudinal study in a rat external fixation model.

In: Biomaterials Science. Vol. 10 (2022) 6, 1532 - 1543.

First published online by RSC: 10.02.2022

https://dx.doi.org/10.1039/D2BM00051B

Dynamic *in vivo* monitoring of fracture healing process in response to magnesium implant with multimodal imaging: Pilot longitudinal study in a rat external fixation model.

Yu Sun[a, b], Heike Helmholz[a], Olga Will[c], Timo Damm[c], Björn Wiese[a], Monika Luczak[a], Eva Peschke[c], Bérengère Luthringer-Feyerabend[a], Thomas Ebel[a], Jan-Bernd Hövener[c], Claus-Christian Glüer[c], Regine Willumeit-Römer[a]

[a] Institute of Metallic Biomaterials, Helmholtz-Zentrum Hereon, Geesthacht 21502, Germany;
[b] Department of Orthopaedics, First Hospital of China Medical University, Shenyang 110001, China;
[c] Molecular Imaging North Competence Center (MOIN CC), Section Biomedical Imaging, University Hospital Schleswig-Holstein (UKSH), Kiel University (CAU), Kiel 24118, Germany.

Correponding author: Yu Sun (Email: yu.sun@hereon.de)
Given name: Yu
Family Name: Sun
Telephone: (+49)1748275127; (+86)13609815765.

Author: Heike Helmholz (Email: heike.helmholz@hereon.de)
Given name: Heike
Family Name: Helmholz

Author Olga Will (Email: olga.will@rad.uni-kiel.de)
Given name: Olga
Family Name: Will

Author: Timo Damm (Email: timo.damm@rad.uni-kiel.de)
Given name: Timo
Family Name: Damm

Author: Björn Wiese (Email: bjoern.wiese@hereon.de)
Given name: Björn
Family Name: Wiese

Author: Monika Luczak (Email: monika.luczak@hereon.de)
Given name: Monika
Family Name: Luczak

Author: Eva Peschke (Email: Eva.Peschke@rad.uni-kiel.de)
Given name: Eva
Family Name: Peschke

Author: Bérengère Luthringer-Feyerabend (Email: berengere.luthringer@hereon.de)
Given name: Bérengère
Family Name: Luthringer-Feyerabend

Author: Thomas Ebel (Email: thomas.ebel@hereon.de)
Given name: Thomas
Family Name: Ebel

Author: Jan-Bernd Hövener (Email: jan.hoevener@rad.uni-kiel.de)
Given name: Jan-Bernd
Family Name: Hövener

Author: Claus-Christian Glüer (Email: glueer@rad.uni-kiel.de)
Given name: Claus-Christian
Family Name: Glüer

Author: Regine Willumeit-Römer (Email: regine.willumeit@hereon.de)
Given name: Regine
Family Name: Willumeit-Römer

Abstract

Rodent models are commonly used in pre-clinical research of magnesium (Mg) -based and other types of biomaterials for fracture treatment. Most studies selected unstable fixation methods, and there is a lack of multimodal longitudinal *in vivo* monitoring of bone healing. The purpose of this study is to develop a rat femoral fracture model stabilized by external fixation with intra-medullary Mg implant, and to investigate the dynamic bone union process with several imaging techniques offering complementing insights into the process. Pure Mg pins were prepared, followed by in vitro degradation test. Male Sprague-Dawley rats in the experimental group underwent femoral osteotomy stabilized by external fixators with intra-medullary implantation of Mg pins, and the control group underwent external fixation without intra-medullary implants. Post-operative radiograph, micro-CT and B-mode ultrasonography were acquired directly after surgery, and re-examined at week 4, 8 and 12. Bone tissue volume, *in vivo* implant degradation, histological staining and MRI images were analyzed using *ex vivo* samples. Both groups achieved fracture union at week 12, and the dynamic healing process was illustrated by *in vivo* radiograph, micro-CT and ultrasonography. Bilateral whole femur *ex vivo* analysis further demonstrated increased ratio of bone tissue volume in the surgical femur with Mg implants, and *in vivo* degradation of Mg pins was slower than *in vitro* results. Titanium screws rather than intra-medullary Mg pins were the source of artifact in MRI. This pilot study showed the rat fracture model with external fixation and intra-medullary Mg implantation, to be an effective method for dynamic *in vivo* monitoring of the bone healing process. Future application of the animal model may facilitate pre-clinical translational research of biodegradable orthopaedic implant materials for fracture treatment.

Keywords: magnesium; implant; fracture; external fixation; multimodal imaging.

1. Introduction

Magnesium (Mg) -based biodegradable materials are promising candidates for the manufacturing of medical implants, with broad potential indications for clinical treatment of musculoskeletal diseases, especially bone fractures at various anatomical sites.[1-4] In comparison with traditional metal materials such as stainless steel (SS) and titanium (Ti), the elastic modulus of Mg-based alloys is closer to that of cortical bone and reduces the stress-shading effects.[5-7] The degradation characteristics of Mg-based materials also lowers the risks associated with secondary surgeries for implant removal, such as postoperative infection and neurovascular damage.[8] Besides, compared with Ti and steel, Mg and its alloys may produce less pronounced interference artifacts caused by beam hardening during X-ray and computed tomography (CT) examination, thus permitting accurate diagnosis and post-operative evaluation for clinical follow-up.[9]

However, due to the degradation after implantation, there are concerns on safety and mechanical stability of Mg-based medical devices, which is essential for early stage of fracture healing at weight-bearing sites such as femur and tibia.[10] To solve the problem, new alloys were developed to tailor both mechanical and degradation properties, various surface treatment methods have been tested, and new structural design should be considered for Mg-based devices to endure high torque for clinical application.[11] Moreover, the strategy of using hybrid system for fracture treatment at weight-bearing sites has become a novel research direction, in which the tradition metallic components provide long-term reliable mechanical support and Mg-based components promote bone formation via degradation products.[10, 12] In recent years, numerous *in vitro*, *in vivo* and clinical studies have demonstrated the biological benefits of Mg-based materials in promoting osteogenesis as stand-alone implants or as part of hybrid systems.[2, 3, 13-16] These advantages, application strategies and success led to more research in developing novel biodegradable materials for clinical applications.[13, 17, 18]

For novel biomaterials or treatment methods, pre-clinical studies based on small and large animal models are critical for the successful translation into clinical applications.[19, 20] In comparison with Ti and SS, for Mg-based biomaterials, animal studies could be more essential for investigation of toxicity and corrosion, considering the partly contradictory results between *in vitro* and *in vivo* studies.[21-26] In general, small animals (rodents) could be selected for evaluation of biocompatibility as well as degradation and local tissue response after implantation,[24, 27, 28] and large models such as sheep and pigs are used to document clinical efficacy by allowing application of medical devices with the same dimension for human surgery.[29-32] However,

experiments with large lab animals are more expensive, time- and space-consuming, and might be infeasible when a large sample size is required. Although the small body size of rodents poses difficulties for both surgical simulation and device preparation, rats and mice are relatively easy to handle and to keep in large quantities. Besides, with a considerable variety of biological reagents such as antibodies available, and easy access to high-resolution imaging modalities such as micro-CT, rodents are commonly selected lab animal species in studies of biomaterials for investigation of biological mechanism.[19, 20] These advantages encourage developing novel *in vivo* rodent models simulating the clinical pathological conditions and treatment methods, to provide convincing pre-clinical evidence for developing implant materials.

The complex and dynamic degradation process of Mg-based biomaterials is the key factor determining their unique biological effects on bone formation.[13, 18] To investigate these effects, previous studies used *in vitro* tests with or without cell culture, or non-fracture *in vivo* rodent models such as intramedullary implantation to explore the biological mechanism.[17, 27, 33-35] Although rodents are relatively convenient to keep in large number with a short experimental cycle, the previous research using simple surgical designs had limitations in simulating the drastic changes in cellular components, local tissue environment, and systematic metabolic status during the orchestrated fracture healing process.[36]

The authors' previous systematic review revealed that rodents were the most commonly used species for pre-clinical *in vivo* fracture research of Mg implants, and rats have been selected more frequently than mice.[37] Among the studies with rat models, Mg and its alloys were used either independently or within a hybrid system to support fracture healing, but all studies selected intra-medullary pins or nails without locking mechanism for fracture fixation.[12, 38-43] Due to the lack of axial and rotational stability, the post-operative four-limb weight-bearing might be delayed, and notably, the influence of fixation instability on callus formation and bone healing was revealed by previous studies in rodents, which will be a confounding factor for interpretation of research results.[44-49] Besides, the application of intramedullary Mg implants may lead to re-fracture due to mechanical failure prior to bone union, thus not allow for effective monitoring of the entire fracture healing process.[12] As to other surgical methods, external fixation devices could be a reasonable choice for rodents, and have been used in previous research on distraction osteogenesis (DO) in rats, similar to the common fracture model. However, in previous publications major components of DO fixators were prepared with metallic materials, which will result in severe artifacts for *in vivo* micro-CT analysis.[50-52] Moreover, most studies on Mg-based materials in rat fracture models were cross-sectional in study design, requiring sacrifice of animals for sample harvesting at multiple time points. This increases the number of animals needed,[39, 40, 42, 51, 52] and it does not permit

continual monitoring with imaging methods such as micro-CT to present the complete fracture healing process in an individual animal. The above technical limitations may lead to discrepancies between pre-clinical evidence and clinical outcome, and more efforts are needed to improve the translational value of rodent fracture models for biomaterials research.

The purpose of this longitudinal study is to develop a rat fracture model using external fixation device with relevance for clinical translation, also as a novel hybrid system for investigation of the biological effects of intra-medullary Mg-based implants during the healing process. The strategy of dynamic imaging will allow continual monitoring of disease progression and bone healing in the same experimental animal, thus not only decreasing the inter-individual variation and number of animals as promoted by the 3R principle,[53] but also better simulating the clinical post-operative follow-up of patients undergoing orthopaedic surgeries.

2. Materials and methods

2.1. Surgical design for fracture fixation, Mg implantation and imaging

The authors designed a rat femoral fracture model stabilized by external fixation device with intra-medullary pin implantation, for evaluation of the bone healing process in response to Mg implants (Fig. 1, Fig. 2a-f). In this model, cylindrical pins made from pure Mg were implanted into the intramedullary cavity after fracture induction, and external fixators (RatExFix, RISystem AG, Switzerland) composed of 1 PEEK connection bar and 4 titanium (Ti) screws,[54] were used for stabilization to support bone healing (Fig. 2g-2h). The PEEK bar allows acquiring micro-CT images without metal artifact (Fig.2i-2j) in a region of interest surrounding the fracture line. The fixator was also used as a fixed landmark for registration of post-operative CT and ultrasonography images.

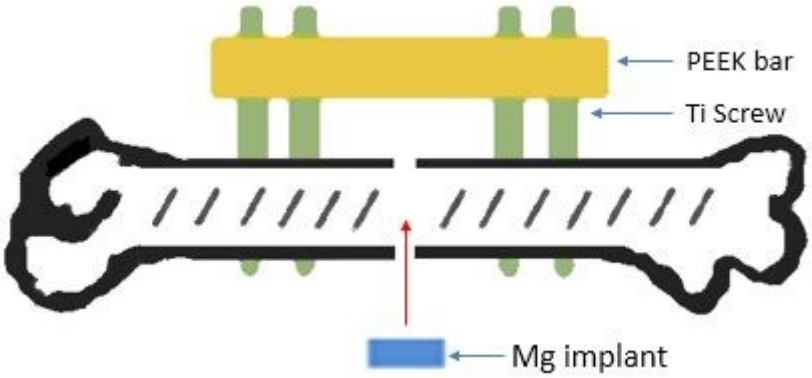

Figure 1. External fixation of femoral fracture and intra-medullary Mg pin implantation.

Titanium screws were used for fracture fixation via a connection bar made from PEEK, and a pure Mg pin was inserted as an intra-medullary implant.

2.2. Mg implant preparation

Pure Mg pins, with a diameter of 1.2 mm and length of 5.0 mm (Fig. 2g), were prepared by permanent mold casting of pure (99.99%) Mg granules followed by extrusion procedures. Pure Mg (99.985%, MAGONTEC, Sydney, Australia) was melted and kept at 720 °C. Protective gas (Ar + 3 volume-% SF6) was applied during the melting and casting process. The melt was poured into a mild steel mold preheated to 650 °C and held in a furnace for at least 5 minute and quenched in water at room temperature in a controlled manner, which is known as direct chill casting. The ingots were machined to a length of 150 mm and a diameter of 49 mm. The ingots were preheated for 1 h prior to indirect extrusion at 350 °C. During extrusion, the ram speed was 0.9 mm/s with an extrusion ratio of 1/69.4 from a diameter of 50 mm to 6 mm. The extruded rods were turned into pins with a diameter of 1.2 mm and lengths of 5.0 mm. All prepared Mg pins were weighed for volume calculation and cleaned in ultrasonic bath, then individually packed in airtight plastic bags using a vacuum sealer, and underwent Cobalt-60 gamma-radiation for pre-operative sterilization.

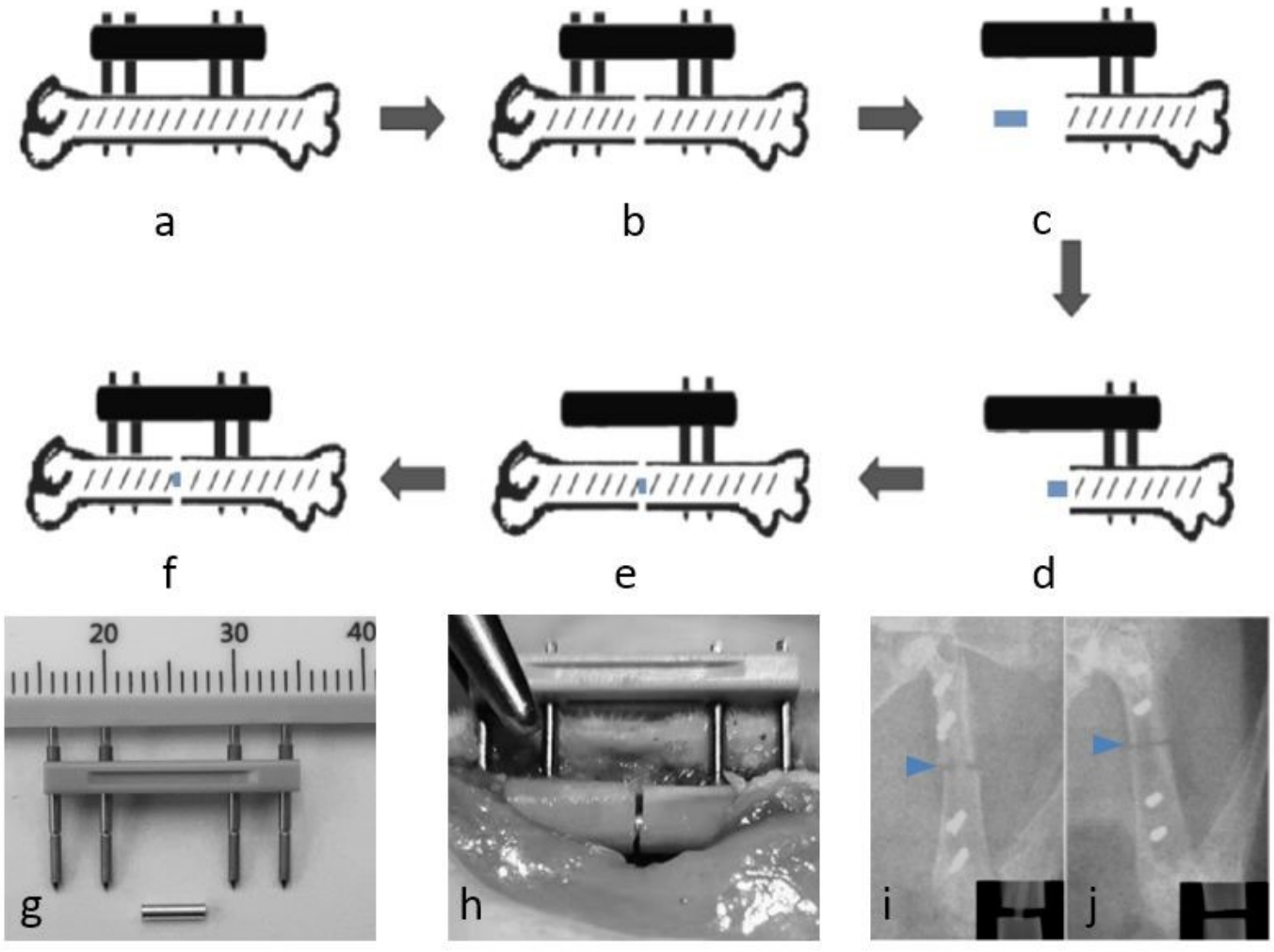

Figure 2. Introduction of the model: surgery, fixation device and Mg implant.
Illustrations showing the surgical procedure:
(a) Mounting of the external fixator;
(b) Fracture induction (osteotomy) using wire saw;
(c) Releasing the distal femur for Mg pin implantation;
(d) Insertion of Mg implant into the medullary cavity;
(e) Fracture reduction;
(f) Mounting screws in distal femur to complete implantation and fixation;
External fixator, Mg implant and identification on post-operative imaging:
(g) External fixator and Mg implant (PEEK bar, Ti screws and pure Mg pin);
(h) Intra-operative view of fracture fixation and intra-medullary implant;
(i-j) Post-operative radiograph and CT images, showing the fracture site (blue arrowheads) and implantation status, as the application of PEEK bar permitted 3D rendering without obvious metal artifact (imaging on the day of surgery, i: pure-Mg group, j: no-Mg group).

2.3. *In vitro* degradation test

In order to investigate possible influence of the titanium screws on the degradation of the Mg-pins, a special experimental setup was used. The *in vitro* degradation experiments involved: (1) 6 Mg pins with Ti screws and (2) 6 Mg pins without Ti screws. For the first setting (pin with screws), each Mg pin was tightened together with 2 Ti screws using a silicon tube (Fig. 3). The pins and screws were incubated in 1 ml DMEM cell culture medium (Gibco, GlutaMAX) containing 10% fetal bovine serum, at cell culture conditions (37°C, 5% CO_2, 95% humidity). Initial weight was determined and compared to the weight after 7 days (168 hours) of incubation after removal of degradation products. The average *in vitro* degradation rate was calculated using the weight differences of 6 independent samples.[55, 56]

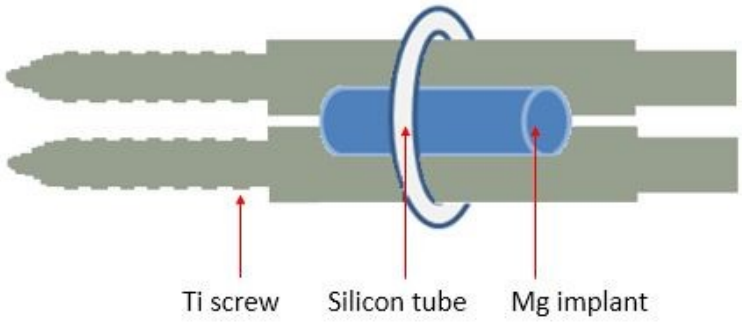

Figure 3. *in vitro* degradation test.

2.4. Animal group setting and experimental plan

The experimental protocol was applied via local authority (Ministry for Energy Transition, Agriculture, Environment, Nature and Digitalization, Schleswig-Holstein, Germany), and 3 male Sprague-Dawley rats were approved in each group for a pilot study with a post-operative follow-up of 12 weeks (application number: V242-30912/2020). Post-operative *in vivo* imaging was

conducted every 4 weeks to monitor the fracture healing process (Fig. 4). The rats (300-350 g at the age of 8 weeks) purchased from Janvier Labs (Saint-Berthevin Cedex, France) were kept in the central animal facility at the author's institution for a 2-week accommodation period before the operation day, with free access to food and water in a 12-hour day-night light cycle. Before surgery the animals were randomly assigned to the experimental and control group, respectively.

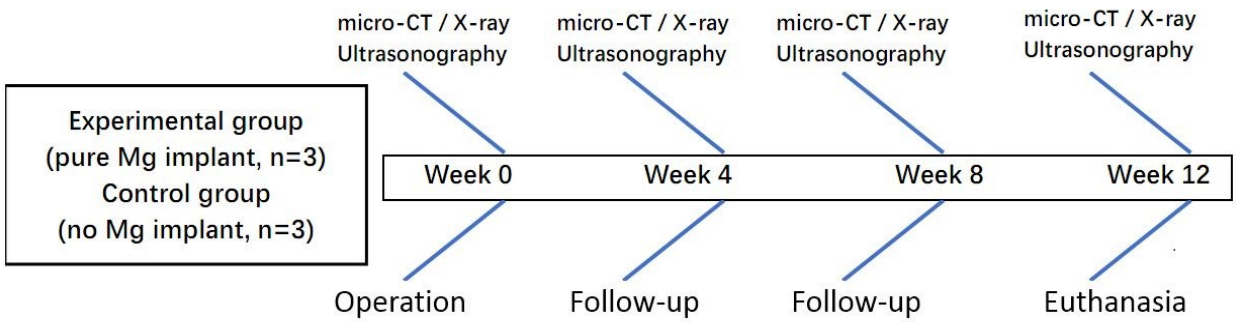

Figure 4. Group setting and experimental timeline.

2.5. Surgical procedure

For general anesthesia of surgery and post-operative imaging, ketamine (75 mg/kg; WDT, Germany) and medetomidine (0.5 mg/kg; Domitor, Orion Pharma, Finland) were administered via intraperitoneal injection. The left hind limb was shaved and treated with skin disinfectant (Kodan forte, Schülke, Germany), and the eyes were protected with eye ointment (Bepanthen, Bayer, Germany). The rats were then placed on an electric blanket (38°C) and covered with a sterile drape.

A 4 cm lateral skin incision was made along the femur, and the underlying muscle groups were separated to expose the femoral shaft. After mounting the external fixator, osteotomy was performed using a 0.66 mm wire saw to induce fracture at the middle level of the fixator. Then the distal femur was released, followed by irrigation with normal saline to remove bone and metal debris, and the pure Mg implant was inserted into the medullary cavity. The implantation of Mg pin was only performed in the experimental group, and no pin implantation was conducted in the control group. The distal femur was then fixed at anatomical position with Ti screws. After fracture fixation, the muscles and skin were sutured with 4-0 absorbable and 3-0 non-absorbable threads respectively. Surgical procedures were performed by an experienced surgeon (Y.S.) with certified training for the external fixation system (more information of surgical steps in Supplementary material. Fig. S1).

No systematic antibiotics was administered and the animals were antagonized with atipamezole (1 ml/kg; Antisedan, Orion Pharma, Finland) subcutaneously to wake-up. Chlorhexidine sprays (Clorexyderm, ICF, Italy) were administered at incision site twice per day for 3 days. For analgesia, 1% lidocaine (Xylocain, Aspen Pharma, Irland) was administered pre-operatively via subcutaneous infiltration injection (100 µl) around incision, metamizol (100 mg/kg; WDT, Germany) was applied subcutaneously before waking up from anesthesia and repeated with a 6-hour interval, and the animals were also treated with tramadol (Tramal, Grünenthal, Germany) in drinking water (0.1 mg/ml) for 5 days.[57] Post-operative observation was continued to monitor the general status, animal behavior, incision healing, air cavity formation and weight-bearing status, with the body weight recorded every 4 weeks.

2.6. Micro-CT

CT scans were conducted using a micro-CT Scanner (vivaCT 80, Scanco Medical AG, Switzerland). *In vivo* scans were performed at a voltage of 70 kVp, beam current of 114 µA, isotropic voxel size of 39 µm, 350 ms integration time, and with 219 slices within the fracture region. The scout-view images for defining the scanning level were also saved as 2D radiographs for longitudinal analysis.

Ex vivo scans were conducted for the following purposes: (1) For evaluation of bone tissue formation, the whole length of bilateral femur samples (surgical side and contralateral non-surgical side) was scanned with the same protocol as for *in vivo* imaging. A global fixed threshold of 270 mgHA/ccm was defined for segmentation of mineralized tissue and quantification of bone tissue volume at the final time point week 12. Then the ratio of bone tissue volume between surgical side and contralateral side was calculated for comparison between groups; (2) For evaluation of the implant degradation with higher resolution, *ex vivo* samples of the surgical limb were further scanned at a voltage of 70 kVp, beam current of 114 µA, isotropic voxel size of 11.6 µm, 500 ms integration time, with the whole implant area included. Semi-automated and manual segmentation was performed for analyzing the volume change of Mg implants and calculation of degradation rates; (3) As a reference for the skeletal structures and implant position on *ex vivo* magnetic resonance imaging (MRI), two rat femur samples (not from the *in vivo* experiments) were scanned using the *in vivo* micro-CT parameters. Fiji (https://imagej.net/Fiji.html), Mango (Research Imaging Institute, University of Texas Health Science Center) and Voxler (Golden Software, USA) were used for qualitative and quantitative analysis of bone tissue volume, implant volume and 3D rendering of the dynamic healing process.[58, 59] *In vivo* degradation rate was calculated according to the implant's volume loss during the 12-week post-operative period.[55, 56]

2.7. B-mode ultrasonography

B-mode ultrasonography examination was conducted using the Vevo 2100 system (VisualSonics; Toronto, ON, Canada) and MS550S probe, with a center frequency of 40 MHz and 25 frames/second data acquisition rate, generating ultrasound images with lateral and axial resolutions of 90 and 40 μm, respectively. The animal was placed on lateral position with the surgical-limb side upward, and the probe was placed parallel to the PEEK bar and anterior to the quadriceps muscle. The following B-mode settings were kept constant during the image acquisition, including gain (70 dB), dynamic range (70 dB) and image depth (10 mm).

2.8. Histology

At the end time-point week 12, after *in vivo* imaging and removal of external fixators, all rats were euthanized via overdose anesthesia through cardiac puncture, and bilateral hind limbs were obtained. The samples were first wrapped using tissue paper soaked with PBS and stored at -20°C. After thawing at 4°C overnight, *ex vivo* micro-CT scans were conducted and the Mg implants were carefully removed to avoid excessive tissue damage. For tissue processing, the samples were stored in 10% neutral buffered formalin as fixation for 72 hours, followed by decalcification in 20% ethylenediaminetetraacetic acid for 10 weeks, with decalcification solution changed every 2 days. After decalcification, the samples were washed with running water for 4 hours and then underwent dehydration in ethanol gradient series, tissue clearing and paraffin embedding. Tissue sections were conducted using a HistoCore Autocut rotary microtome (Leica Microsystems, Germany) with a thickness of 10 μm, and the slides underwent hematoxylin and eosin (H&E) staining for conventional qualitative examination of tissue differentiation and inflammation, using bright-field images taken with a DMi8 microscope (Leica Microsystems, Germany).

2.9. MRI

Two rat femur samples were used for high resolution MRI, to simulate the following surgical methods of *in vivo* rat models respectively: (1) intra-medullary implantation of pure Mg pin without inducing femoral fracture; (2) external fixation of femoral fracture with intra-medullary implantation of Mg pin. The *ex vivo* scans were acquired using a 7 Tesla small animal MR system (BioSpec, Bruker BioSpin, Germany) with a 300 mT/m gradient strength, a transmit/receive volume coil and a receive surface coil. The samples sealed in plastic bags were placed on the animal bed at room temperature, then scanned along the long axis of femur with a T1 RARE sequence (TE 8.09 ms,

TR 791.73 ms, matrix 364 x 364, field of view 60 mm, slice thickness 0.35 mm, 2 averages, bandwidth 240 Hz/px, acquisition time 288 seconds). After MRI, the samples underwent micro-CT scanning using the same parameters of *in vivo* imaging, for localization of anatomical structure and implant position.

2.10. Statistics

Quantitative data were presented as the mean ± standard deviation, with n representing the number of animals. Quantitative results were processed and presented using Microsoft Excel 2016 and SigmaPlot 13. However, as the purpose of this research was to establish a model and the general methods instead of investigating novel materials, and considering the limited sample size approved for this pilot study, no further statistical analysis was performed to detect for significant difference between groups.

3. Results

3.1 Post-operative observation of animal status

There was one anesthesia-related death in the experimental group before wake-up, and the animal was replaced. All other rats survived with good toleration and were not housed in separate cages. The animals returned to four-limb weight bearing and active explorative activities within 2 days, without obvious signs of pain, and the body weight continued increasing during the 12-week follow-up (Supplement material. Fig. S2 and video-clip). One rat had sutures partly removed at day 6 after surgery without signs of infection. The wound was successfully repaired under general anesthesia, but the quantitative *ex vivo* results were not included considering multiple surgeries with prolonged analgesia. All animals' incision healed and the sutures were removed after imaging at week 4, and the PEEK bars were all intact at the end time point. No signs of subcutaneous air cavity formation or severe swelling were observed.

3.2. *In vivo* imaging

In both groups, on radiographs the translucent fracture lines were visible from week 0 to week 8 (Fig. 5a-5c, 5e-5g), and the formation of mineralized callus tissue was already visible on the first follow-up radiographs at week 4 (Fig. 5b, 5f). At week 12, all fractures demonstrated radiographic union, as the osteotomy lines disappeared and continuous bony tissue bridged the distal and proximal fracture sites (Fig. 5d, 5h). In ultrasonography images, the osteotomy lines were clearly visible on week 0 (Fig. 5i, 5m). The bone discontinuity was also distinguishable at week 4 and

week 8 (Fig. 5j-5k, 5n-5o), and finally became invisible at week 12 (Fig. 5l, 5p), reflecting a similar healing trend on radiographs showing increasing newly formed bone tissue over time.

The 3D reconstruction of micro-CT images, in combination with color mapping according to tissue density, presented the dynamic healing process in both groups, as well as the mineralization status of callus tissue over time (Fig. 5q-5x). Because of the difficulty in body positioning due to the dramatically increasing body weight after surgery and a relatively small animal holder, artifacts from adjacent Ti screws were visible (Fig. 5r, 5s, 5w), interfering with more precise quantification of local tissue density at later time points of *in vivo* scans, so the bone tissue volume was only calculated with *ex vivo* micro-CT data after fixator removal.

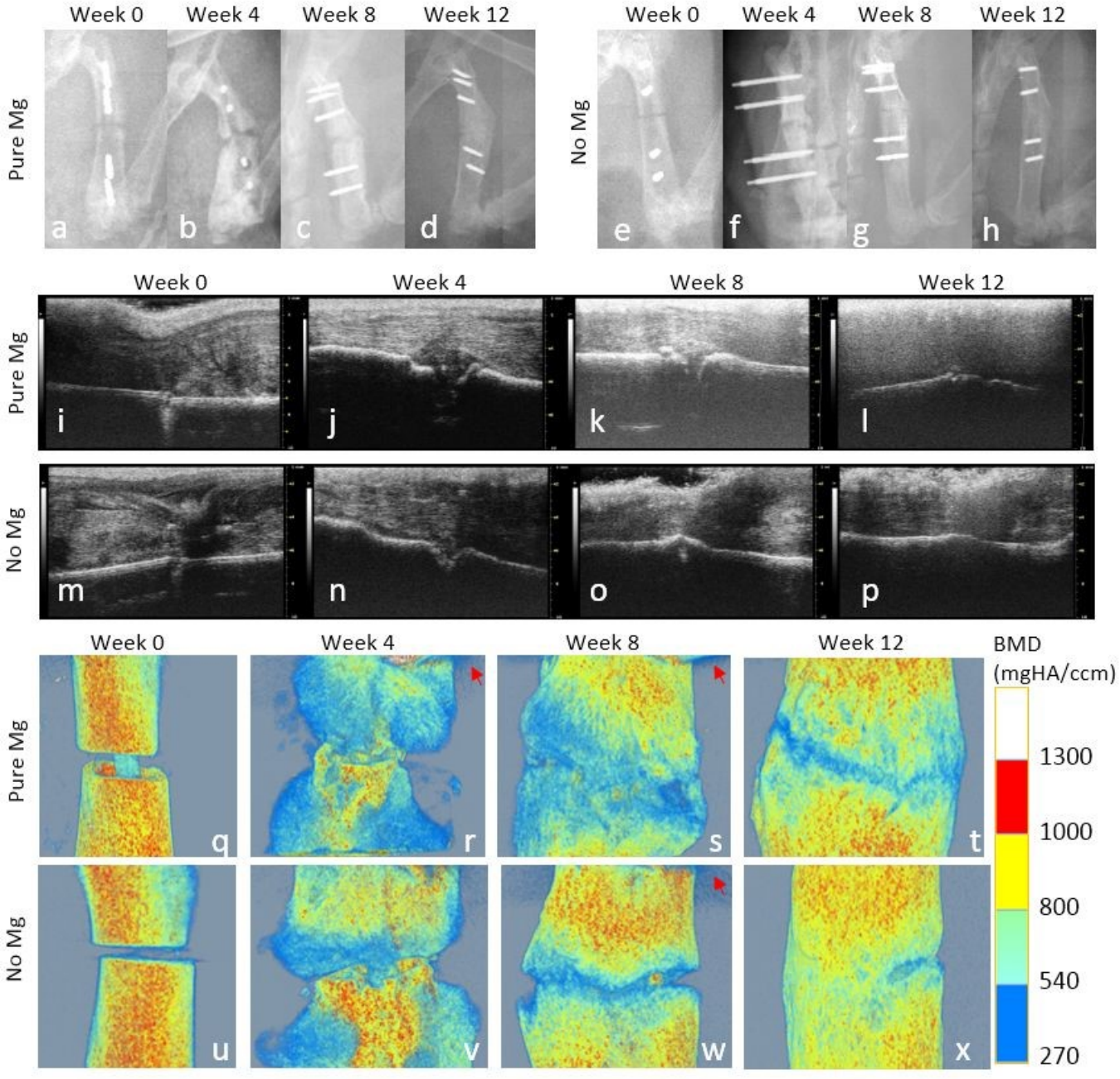

Figure 5. Continuous post-operative *in vivo* imaging from week-0 to week-12.
(a-h) Representative serial radiographs (2D X-ray scout-views from micro-CT device);
(i-p) B-mode ultrasonography of local tissue at the site of osteotomy;
(q-x) 3D reconstruction of micro-CT images with color mapping, illustrating the dynamic mineralization status during bone healing, as well as the process of newly formed bone tissue encapsulating the original femoral shaft during fracture repair.
Note: X-ray scout views (c, d, g) from the micro-CT device showed false proximal "double screws" due to software reasons, but did not interfere with visualization of the fracture site; Red arrows in 3D CT images (r, s, w) indicated the presence of artifact caused by titanium screws.

3.3. Histology and micro-CT imaging of *ex vivo* samples

Macroscopic examination of the harvested femurs confirmed solid fracture healing across the osteotomy gap, as well as the absence of abnormal motion between the distal and proximal parts in all samples. Continuous bone tissue bridging the fracture gaps was further shown by H&E staining, without obvious inflammatory response or scar formation (Fig. 6a-6b). In addition to the above observation, bone union was also demonstrated via 3D reconstruction of CT images (Fig. 6c-6d). The bone tissue volume of bilateral whole femurs was quantified using *ex vivo* micro-CT data and fixed global threshold value. The ratio of bone tissue volume between the surgical femur and non-surgical femur was then calculated, as 127.10 ± 3.97 % in the experimental group and 111.86 ± 7.41 % in the control group (Fig. 6e). The comparison of volume ratio between groups indicated increased bone formation during fracture healing in response to Mg implant, but no further statistical analysis was conducted considering the small sample size in this pilot study.

3.4. *In vitro* and *in vivo* degradation test

The *in vitro* experiment was designed to simulate two extreme settings: (1) Mg pins binding directly to Ti screws, and (2) Mg pins without adjacent Ti screws. The calculated degradation rate was 0.46 ± 0.08 mm/year for Mg implants tested without Ti screws, and 1.11 ± 0.42 mm/year for Mg implants tightened directly with Ti screws. In the animal experiment, Mg pins were placed between the inner two Ti screws instead of direct binding, and the percentage of volume loss after 12-week follow-up was 20.15 ± 3.24 %, with the *in vivo* degradation rate calculated as 0.24 ± 0.04 mm/year based on the volume change of implants from micro-CT data.[55, 56] Degradation of the Mg implants could be visualized on 3D reconstructed images (Fig.6f-6g).

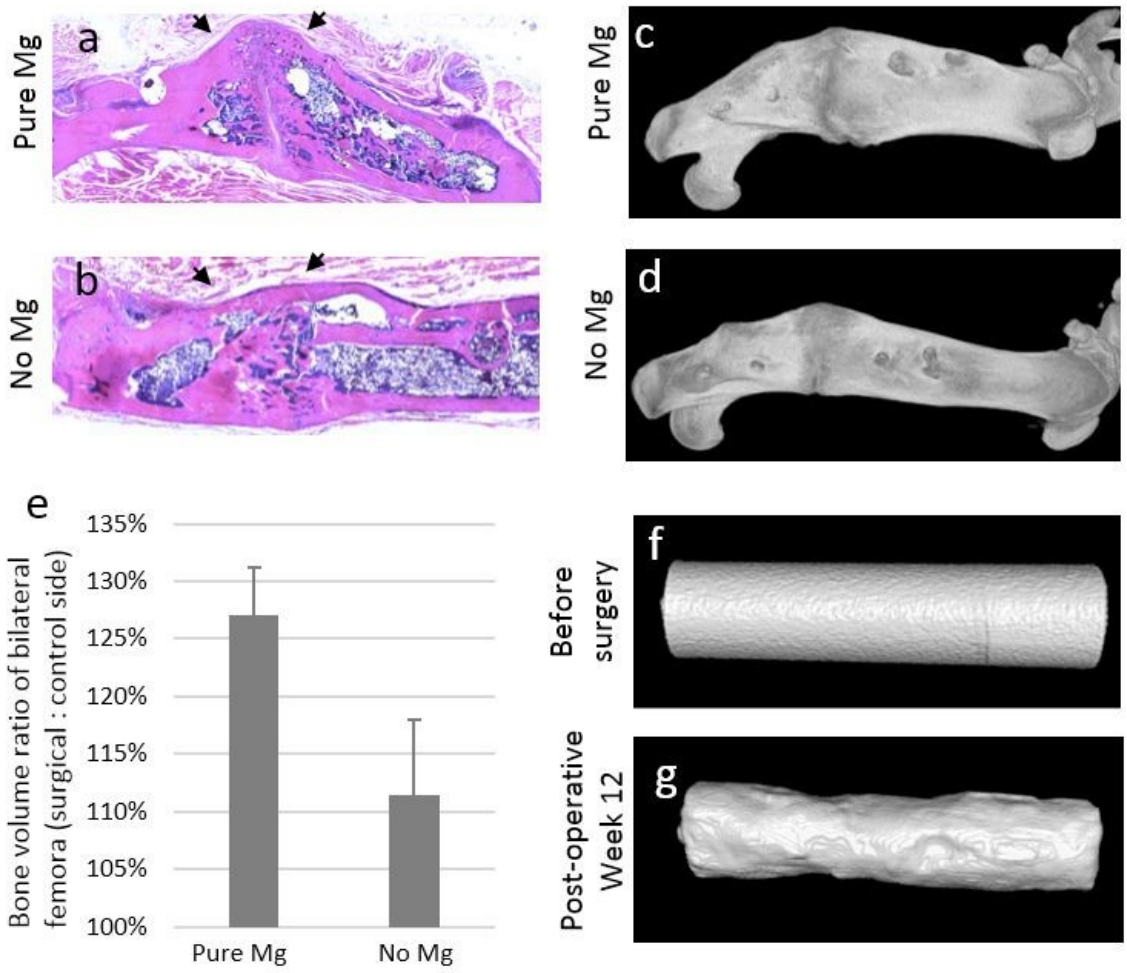

Figure 6. *Ex vivo* imaging, histology and quantitative bone analysis.
(a-b) H&E staining of paraffin embedded samples, demonstrating restoration of femur continuity (arrows);
(c-d) 3D reconstruction of the whole femur on surgical side, after removal of external fixation devices;
(e) Comparison of bone volume ratio between groups, indicating increased bone formation in response to Mg implant;
(f-g) 3D rendering of Mg implant, showing volume change before surgery and at post-operative week 12.

3.5. *Ex vivo* MRI for artifact evaluation

In MR images of the *ex vivo* femur sample without external fixator (Fig. 7a), anatomical details were clearly visualized as in the micro-CT image (Fig. 7b), including the cortical and trabecular structures at the metaphyseal and epiphyseal area. The pure Mg pin as well as the air content was presented as a region with low signal intensity, without obvious artifact disturbing the visualization of adjacent cortex, bone marrow and soft tissue. Micro-CT scan (Fig. 7b) of the same sample further demonstrated the implant position shown on the MRI image. However, for MRI of the other sample with external fixator (Fig. 7c), the anatomical structures were not clearly presented compared with CT images (Fig. 7d), due to the severe artifact caused by Ti screws.

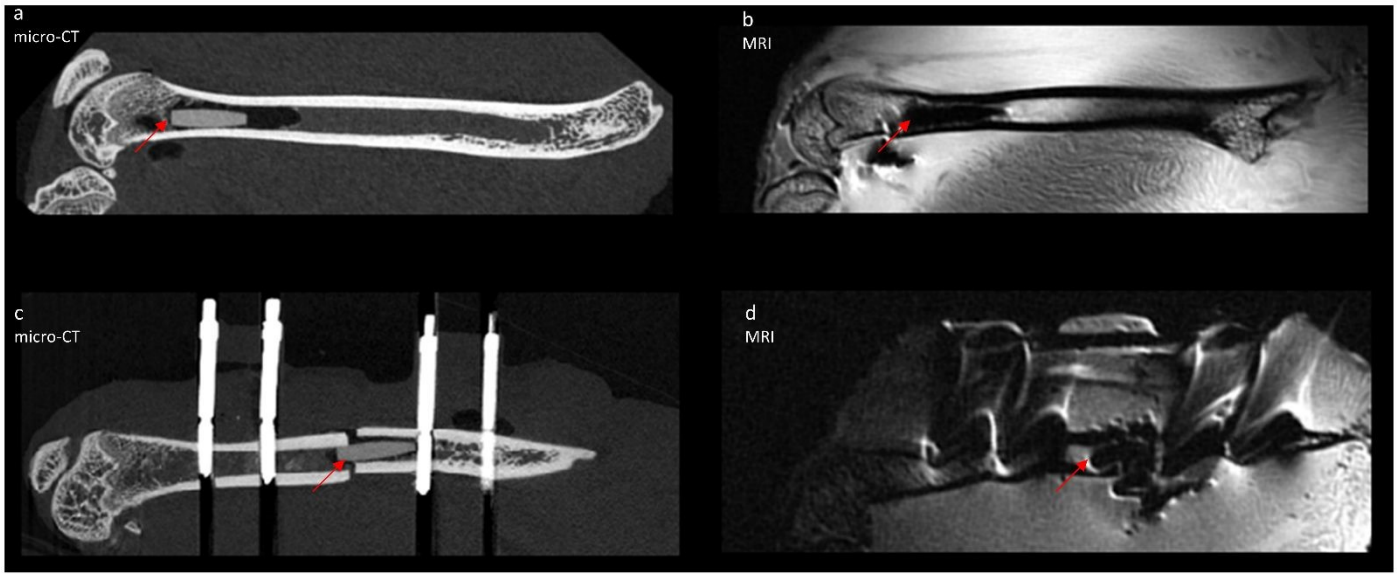

Figure 7. MRI and micro-CT of rat femur samples simulating surgeries.
MRI and micro-CT of the rat femur sample (a-b) with intra-medullary implantation of pure Mg pin, without fixator or fracture; MRI and micro-CT of the femur sample (c-d) with fracture fixation and intra-medullary Mg implant.
Note: the arrows indicate the pure Mg implant in the medullary cavity.

4. Discussion

To develop a pre-clinical rodent fracture model allowing longitudinal *in vivo* imaging, with fixation stability simulating clinical treatment, the authors considered and compared both internal fixation (intramedullary locking nail and plate-screw system) and external fixators. A plate-screw system with 6 Ti screws has the advantage over the external fixator with 4 screws, providing higher overall pull-out strength from cortical bone.[49] Besides, the external fixation may lead to more complications including skin irritation and infection than internal fixation.[60] But the external fixator has the unique advantage that the polymeric connection bar could function as a constant landmark, allowing accurate positioning for CT and ultrasonography. An accurate orientation and rapid preparation will decrease the risk of repetitive positioning for post-operative imaging, and decrease the total time for anesthesia providing better animal safety, which is especially important for our pilot study with a small sample size. As to fixation strength, the external fixator provides standardized stability compared to traditional non-locking intra-medullary nail or pins, with evidence from biomechanical studies.[44, 45, 49, 54, 61-63] This is also supported by the post-operative observation that all animals resumed four-limb weight-bearing activities within 2 days after surgery (Supplementary material. video-clip), and longitudinal *in vivo* imaging was successfully realized.

As an exploratory pilot study to assess the efficacy of a new animal model, pure magnesium was selected as the implant, and the results showed good safety considering the general post-operative status of animals, as well as the absence of adverse muscle tissue reactions. Future

studies may include more types of Mg-based materials, such as alloys with or without coatings, or even extend to other bioactive materials or agents with carrier system, for example, biodegradable zinc alloys or ceramics. As to group setting for future research using the model, the authors suggest a study design with at least 3 categories, including novel materials as the experimental group, pure Mg as the positive control, as well as a negative control without implant or using intra-medullary PEEK pin instead. In addition, our implant with a length of 5mm is easy to handle during surgery. Though a smaller implant size such as 3 mm may increase the surgical difficulty, it will allow a smaller constant region of interest for analysis, with less CT artifact from adjacent Ti screws as well as less scanning time, thus facilitating *in vivo* monitoring of the implant degradation process. The researchers could adjust the implant dimension according to their study purpose and technical parameters.

The post-operative *ex vivo* analysis showed increased bone formation in the pure Mg group, and slower implant degradation compared with *in vitro* test, indicating the potential positive effects of Mg implants on bone healing. Previously published studies revealed the complex mechanisms through which magnesium-based materials may promote bone formation and fracture healing. Jähn et al. showed in a mouse femur fracture model that the degradation products of magnesium alloy could enhance osteoblast function and stimulate callus formation, while exerting an inhibitory effect on osteoclasts, thereby reducing bone resorption.[55] The study by Zhang et al. using a rat intra-medullary implantation model demonstrated that Mg ions released during degradation could upregulate calcitonin gene-related peptide expression in the periosteum region, thus promoting bone formation around cortical bone.[12] In another study involving a rat femur model of distraction osteogenesis, Mg implants improved bone vascularization through activation of the vascular endothelial growth factor signaling.[51] Further studies with multimodal *in vivo* imaging techniques may further reveal the underlying mechanisms through which Mg-based implants will improve fracture healing.

For only 3 animals were approved in each group, the authors did not conduct further statistical analysis based on the results, and there are other limitations in the study that can be improved in future research. The authors applied to use female rats for the project, but only male rats were approved in this pilot study. The male rats continued increasing in body weight to more than 500 g (Supplementary materials, Fig. S2) during the 12-week follow-up, exceeding normal capacity of the animal holder for micro-CT device and leading to increased difficulty in proper orientation for artifact control. As female rats are generally smaller in body weight, the authors suggest to select female Sprague-Dawley or other rat species less than 400 g during post-operative follow-up, when

in vivo micro-CT over longer time periods is planned and only smaller holders are available. Besides, female rats were also recommended and frequently used in published studies of fracture healing with Mg implants,[20, 64] thus the selection of female gender also facilitate comparison with previous research. As to sample processing, tissue damage was unavoidable during the removal of intra-medullary implants, causing difficulties in obtaining large number of high-quality tissue sections for further qualitative and quantitative analysis, so the authors suggest to select plastic embedding of non-decalcified samples and hard-tissue sectioning in future studies.[12, 40-42, 55]

In addition, the study selected radiographs, micro-CT and ultrasonography for *in vivo* imaging. The authors suggest to include more continuous imaging or non-imaging modalities in future similar studies, such as photoacoustics, fluorescence imaging and biochemical or biomechanical analysis.[65-69] The test with *ex vivo* samples suggested that Ti screws were the major source of MRI artifact, which is not unexpected because of the field distortions caused by Ti. Specialized sequences may be used to partially address the problem, and dynamic MRI with multiple sequences could be realized by using non-metallic screws.[70] Still, the authors suggest a preemptive MRI test to check if the implant material to be tested could be another source of artifact. Further details of potential applications and extensions of the current model are listed in Figure 8.

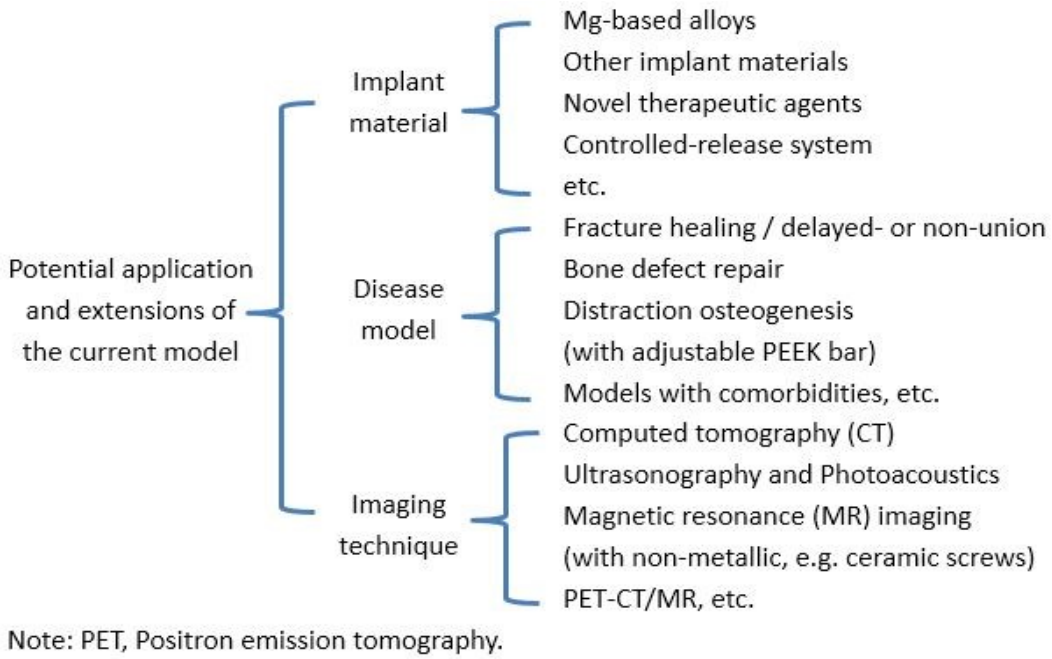

Figure 8. Potential application and possible extensions of the model in pre-clinical research.

5. Conclusions

This pilot study showed that a rat femur fracture model with external fixation and intramedullary Mg implant, could be a safe design to support bone healing and an insightful method for dynamic *in vivo* monitoring of the complex bone healing process. Post-operative analysis showed increased bone formation with Mg implantation, and *in vivo* degradation of Mg was slower than *in vitro* tests. The model facilitates the time-dependent continuous analysis of the biological effects of intramedullary Mg implants, and its feasibility enables extended application for preclinical research of novel biomaterials or fracture treatment approaches.

Conflicts of interest

There are no conflicts of interest to declare.

Acknowledgment

The authors express sincere thanks to our colleagues and collaborators for their kind support:
Professor Dr.Gerhard Schultheiß, Sarah Vieten and ZTH team (Central animal facility, Kiel University (CAU), Kiel, Germany);
Prof. Håvard Haugen and Dr. Catherine Heyward (Institute of Clinical Dentistry, University of Oslo), as well as Dr. Jithin Jose and Joost Holthof (FUJIFILM VisualSonics) who are partners in the MgSafe project (European Union's Horizon 2020 research and innovation program under the Marie Skłodowska-Curie grant agreement No 811226);
Dr. Jana Humbert, Jaime Peña and Gabriele Trompke (MOINCC, Section Biomedical Imaging, UKSH, Kiel University (CAU), Kiel, Germany);
Dr. Liudmila Britanova, Dr. Berit Zeller-Plumhoff, Dr. Katharina Philipp, Annette Havelberg and Anke Schuster (Institute of Metallic Biomaterials, Helmholtz-Zentrum hereon);
Yu-wen Zhang (zoe_ywz@instagram, artist support of graphical work).
The MOIN CC infrastructure was made possible by a grant from the state of Schleswig-Holstein and the European Union ERDF-European Regional Development Fund (Zukunftsprogramm Wirtschaft).

List of Abbreviations

Mg	Magnesium
Ti	Titanium
SS	Stainless steel
PEEK	Polyether ether ketone
3R	Replace, Reduce, Refine
CT	Computed tomography
MRI	Magnetic resonance imaging
BMD	Bone mineral density
H&E staining	hematoxylin and eosin staining

Reference

1. H. Windhagen, K. Radtke, A. Weizbauer, J. Diekmann, Y. Noll, U. Kreimeyer, R. Schavan, C. Stukenborg-Colsman and H. Waizy, Biomedical engineering online, 2013, 12, 62.

2. O. Kose, A. Turan, M. Unal, B. Acar and F. Guler, Archives of orthopaedic and trauma surgery, 2018, 138, 1069-1075.

3. X.B. Yu, D.W. Zhao, S.B. Huang, B.J. Wang, X.Z. Zhang, W. Wang and X. Wei, BMC Musculoskeletal Disord., 2015, 16, 329.

4. A. Gigante, N. Setaro, M. Rotini, S.S. Finzi and M. Marinelli, Injury, 2018, 49, Suppl 3:S48-S53.

5. F. Witte, Acta Biomater., 2010, 6, 1680-1692.

6. A.K. Gartzke, S. Julmi, C. Klose, A.C. Waselau, A. Meyer-Lindenberg, H.J. Maier, S. Besdo and P. Wriggers, J. Mech. Behav. Biomed. Mater., 2020, 101, 103411.

7. F. Rezaei, K. Hassani, N. Solhjoei and A. Karimi, Australas. Phys. Eng. Sci. Med., 2015, 38, 569-580.

8. R. Biber, J. Pauser, M. Brem and H.J. Bail, Trauma case reports, 2017, 8, 11-15.

9. P. Stradiotti, A. Curti, G. Castellazzi and A. Zerbi, European spine journal, 2009, 18, Suppl 1:102-108.

10. L. Tian, Y.F. Sheng, L. Huang, D.H.K. Chow, W.H. Chau, N. Tang, T. Ngai, C. Wu, J. Lu and L. Qin, Biomaterials, 2018, 181, 307-309.

11. J.L. Wang, J.K. Xu, C. Hopkins, D.H.K. Chow and L. Qin, Adv. Sci. (Weinheim, Ger.), 2020, 7, 1902443.

12. Zhang Y, Xu J, Ruan YC, Yu MK, O'Laughlin M, Wise H, D. Chen, L. Tian, D. Shi, J. Wang, S. Chen, J.Q. Feng, D.H.K. Chow, X. Xie, L. Zheng, L Huang, S. Huang , K. Leung, N. Lu, L. Zhao, H. Li, D. Zhao, X. Guo, K. Chan, F. Witte, H.C. Chan, Y. Zheng and L. Qin, Nat. Med. (N. Y., NY, U. S.), 2016, 22, 1160-1169.

13. F. Witte, V. Kaese, H. Haferkamp, F. Switzer, A. Meyer-Lindenberg, C.J. Wirth and H. Windhagen, Biomaterials, 2005, 26, 3557-3563.

14. J. Levorova, J. Duskova, M. Drahos, R. Vrbova, D. Vojtech, J. Kubasek, M. Bartos, L. Dugova, D. Ulmann and R. Foltan, J. Biomater. Appl., 2018, 32, 886-895.

15. R. Willumeit, A. Mohring and F. Feyerabend, Int J Mol Sci., 2014, 15, 7639-7650.

16. D. Zhao, F. Witte, F. Lu, J. Wang, J. Li and L. Qin, Biomaterials, 2017, 112, 287-302.

17. A. Chaya, S. Yoshizawa, K. Verdelis, N. Myers, B.J. Costello, D.T. Chou, S. Pal, S. Maiti, P.N. Kumta and C. Sfeir, Acta Biomater., 2015, 18, 262-269.

18. M.M. Gawlik, B. Wiese, V. Desharnais, T. Ebel and R. Willumeit-Romer, Materials, 2018, 11, 2561.

19. M. Peric, I. Dumic-Cule, D. Grcevic, M. Matijasic, D. Verbanac, R. Paul, L. Grgurevic, V. Trkulja, C.M. Bagi and S. Vukicevic, Bone, 2015,70, 73-86.

20. T. Histing, P. Garcia, J.H. Holstein, M. Klein, R. Matthys, R. Nuetzi, R. Steck, M.W. Laschke, T. Wehner, R. Bindl, S. Recknagel, E.K. Stuermer, B. Vollmar, B. Wildemann, J. Lienau, B. Willie, A. Peters, A. Ignatius, T. Pohlemann, L. Claes and M.D. Menger, Bone, 2011, 49, 591-599.

21. J. Fischer, D. Profrock, N. Hort, R. Willumeit and F. Feyerabend, Mater Sci Eng B-Adv., 2011, 176, 830-834.

22. J. Wang, F. Witte, T. Xi, Y. Zheng, K. Yang, Y. Yang, D. Zhao, J. Meng, Y. Li, W. Li, K. Chan and L. Qin, Acta Biomater., 2015, 21, 237-249.

23. L. Scheideler, C. Fuger, C. Schille, F. Rupp, H.P. Wendel, N. Hort, H.P. Reichel and J. Geis-Gerstorfer, Acta Biomater., 2013, 9, 8740-8745.

24. D. Dziuba, A. Meyer-Lindenberg, J.M. Seitz, H. Waizy, N. Angrisani and J. Reifenrath, Acta Biomater., 2013, 9, 8548-8560.
25. C. Rossig, N. Angrisani, P. Helmecke, S. Besdo, J.M. Seitz, B. Welke, N. Fedchenko, H. Kock and J. Reifenrath, Acta Biomater., 2015, 25, 369-383.
26. F. Witte, J. Fischer, J. Nellesen, H.A. Crostack, V. Kaese, A. Pisch, F. Beckmann and H. Windhagen, Biomaterials, 2006, 27, 1013-1018.
27. T. Kraus, S.F. Fischerauer, A.C. Hanzi, P.J. Uggowitzer, J.F. Loffler and A.M. Weinberg, Acta Biomater., 2012, 8, 1230-1238.
28. D. Tie, R. Guan, H. Liu, A. Cipriano, Y. Liu, Q. Wang Q, Y. Huang and N. Hort, Acta Biomater., 2016, 29, 455-467.
29. B. Schaller, J.P.M. Burkhard, M. Chagnon, S. Beck, T. Imwinkelried and M. Assad, Journal of Oral and Maxillofacial Surgery, 2018, 76, 2138-2150.
30. H. Naujokat, J.M. Seitz, Y. Acil, T. Damm, I. Moller, A. Gulses and J. Wiltfang, Acta Biomater., 2017, 62, 434-445.
31. H. Naujokat, C.B. Ruff, T. Kluter, J.M. Seitz, Y. Acil and J. Wiltfang, International Journal of Oral and Maxillofacial Surgery, 2020, 49, 272-283.
32. X.D. Kong, L. Wang, G.Y. Li, X.H. Qu , J.L. Niu, T.T. Tang, K. Dai, G. Yuan and Y. Hao, Mater. Sci. Eng., C, 2018, 86, 42-47.
33. C. Castellani, R.A. Lindtner, P. Hausbrandt, E. Tschegg, S.E. Stanzl-Tschegg, G. Zanoni, S. Beck and A.M. Weinberg, Acta Biomater., 2011, 7, 432-440.
34. H.K. Lim, S.H. Byun, J.Y. Lee, J.W. Lee, S.M. Kim, S.M. Lee, H.E. Kim and J.H. Lee, J. Biomed. Mater. Res., Part B, 2017, 105, 1636-1644.
35. B. Schaller, N. Saulacic, T. Imwinkelried, S. Beck, E.W.Y. Liu, J. Gralla J, K. Nakahara, W. Hofstetter and T. Iizuka, Journal of Cranio-Maxillofacial Surgery, 2016, 44, 309-317.
36. A. Schindeler, M.M. McDonald, P. Bokko and D.G. Little, Semin. Cell Dev. Biol., 2008, 19, 459-466.
37. Y. Sun, H. Helmholz and R. Willumeit, J. Magnesium Alloys, 2021, 9, 351-361.
38. P. Neacsu, A.I. Staras, S.I. Voicu, I. Ionascu, T. Soare, S. Uzun, V.D. Cojocaru, A.M. Pandele, S.M. Croitoru, F. Miculescu, C. M. Cotrut, I. Dan and A. Cimpean, Materials, 2017, 10, 686.
39. D. Li, K. Yu, T. Xiao, Y. Dai, L. Liu, H. Li, D. Jiang and L. Xiong, J. Cell. Physiol., 2019, 234, 21316-30.
40. D.T. Chou, D. Hong, S. Oksuz, R. Schweizer, A. Roy, B. Lee, P. Shridhar, V. Gorantla and P.N. Kumta, J. Biomater. Appl., 2019, 33, 1178-1194.
41. C. Iglesias, O.G. Bodelon, R. Montoya, C. Clemente, M.C. Garcia-Alonso, J.C. Rubio and M.L. Escudero, Biomed. Mater. (Bristol, U. K.), 2015, 10, 025008.
42. G. Li, L. Zhang, L. Wang, G. Yuan, K. Dai, J. Pei and Y. Hao, Acta Biomater., 2018 , 6, 486-500.
43. R. Montoya, C. Iglesias, M.L. Escudero and M.C. Garcia-Alonso, Mat Sci Eng C-Mater, 2014, 41, 127-133.
44. B.M. Willie, R. Blakytny, M. Glockelmann, A. Ignatius and L. Claes, Clin. Orthop. Relat. Res., 2011, 469, 3094-3101.
45. L. Claes, R. Blakytny, J. Besse, C. Bausewein, A. Ignatius and B. Willie, Journal of Orthopaedic Trauma, 2011, 25, 169-74.
46. T. Histing, J.H. Holstein, P. Garcia, R. Matthys, A. Kristen, L. Claes, M.D. Menger and T. Pohlemann, J. Orthop. Res., 2009, 27, 1152-1156.
47. J.H. Holstein, M.D. Menger, U. Culemann, C. Meier and T. Pohlemann, Journal of biomechanics, 2007, 40, 215-219.

48. L.E. Claes, C.A. Heigele, C. Neidlinger-Wilke, D. Kaspar, W. Seidl, K.J. Margevicius and P. Augat, Clin. Orthop. Relat. Res., 1998, 355, S132-147.
49. N. Meyers, M. Sukopp, R. Jager, M. Steiner, R. Matthys, B. Lapatki, A. Ignatius and L. Claes, Plos One, 2017, 12, e0176735.
50. J.L. Wang, J.K. Xu, C. Hopkins, D.H. Chow and L. Qin, Adv. Sci. (Weinheim, Ger.), 2020, 7, 1902443.
51. M. Hamushan, W. Cai, Y. Zhang, T. Lou, S. Zhang, X. Zhang, P. Cheng, C. Zhao and P. Han, Journal of biomaterials applications, 2020, 35, 224-236.
52. M. Hamushan, W. Cai, Y. Zhang, Z. Ren, J. Du, S. Zhang, C. Zhao, P. Cheng, X. Zhang, H. Shen and P. Han, Bioact. Mater., 2021, 6, 1563-1574.
53. V.A. Hampshire and S.H. Gilbert, Toxicol. Pathol., 2019, 47, 329-338.
54. V. Glatt and R. Matthys, J. Visualized Exp., 2014, e51558.
55. K. Jähn, H. Saito, H. Taipaleenmaki, A. Gasser, N. Hort, F. Feyerabend, H. Schlüter, J.M. Rueger, W. Lehmann, R. Willumeit-Römer and E. Hesse, Acta Biomater., 2016, 36, 350-360.
56. ASTM G31-72(2004), Standard Practice for Laboratory Immersion Corrosion Testing of Metals, ASTM International, West Conshohocken, PA, 2004.
57. A. Lang, A. Schulz, A. Ellinghaus and K. Schmidt-Bleek, Lab. Anim., 2016, 50, 433-441.
58. J. Schindelin, I. Arganda-Carreras, E. Frise, V. Kaynig, M. Longair, T. Pietzsch T, C. Rueden, S. Saalfeld, B. Schmid, J.Y. Tinevez, D.J. White, V. Hartenstein, K. Eliceiri, P. Tomancak and A. Cardona, Nature methods, 2012, 9, 676-682.
59. C.A. Schneider, W.S. Rasband and K.W. Eliceiri, Nat. Methods, 2012, 9, 671-675.
60. A. Hadeed, R.L. Werntz and M. Varacallo, External Fixation Principles and Overview, StatPearls. Treasure Island (FL), 2021.
61. V. Glatt, C.H. Evans and R. Matthys, Eur. Cells Mater., 2012, 23, 289-299.
62. E.K .Bliven, M. Greinwald, S. Hackl and P. Augat, Injury, 2019, 50, Suppl 1 S10-S7.
63. H. Hedin and S. Larsson, Injury, 2004, 35, 1255-1263.
64. P. Strube, M. Mehta, A. Baerenwaldt, J. Trippens, C.J. Wilson, A. Ode, C. Perka, G.N. Duda and G. Kasper, Bone, 2009, 45, 1065-1072.
65. R.C.W. Wong, H. Tideman, M.A.W. Merkx, J. Jansen, S.M. Goh and K. Liao, International Journal of Oral and Maxillofacial Surgery, 2011, 40, 393-400.
66. M.R. Forwood and C.H. Turner, Bone, 1995, 17, S197-S205.
67. J.H. Holstein, P. Garcia, T. Histing, A. Kristen, C. Scheuer, M.D. Menger and T. Pohlemann, Journal of Orthopaedic Trauma, 2009, 23, S31-S38.
68. S. Jain and P. Camacho, Curr. Opin. Endocrinol., Diabetes Obes., 2018, 25, 366-372.
69. M.B. Greenblatt, J.N. Tsai and M.N. Wein, Clin. Chem. (Washington, DC, U. S.), 2017, 63, 464-474.
70. N. Schmitz , M. Timmen, K. Kostka, V. Hoerr, C. Schwarz, C. Faber, U. Hansen, R. Matthys, M.J. Raschke and R. Stange, Sci. Rep., 2020, 10, 16238.